Comparison of NMR Solution Structures of the Receptor Binding Domains of *Pseudomonas aeruginosa* Pili Strains PAO, KB7, and PAK: Implications for Receptor Binding and Synthetic Vaccine Design[†,‡]

A. Patricia Campbell, Campbell McInnes, Robert S. Hodges, and Brian D. Sykes*

Protein Engineering Network of Centers of Excellence, 713 Heritage Medical Research Building, University of Alberta, Edmonton, Alberta T6G 2S2, Canada

Received May 12, 1995; Revised Manuscript Received August 28, 1995[⊗]

ABSTRACT: The solution structures of peptide antigens from the receptor binding domains of *Pseudomonas aeruginosa* strains PAO and KB7 have been determined using two-dimensional ^{1}H NMR techniques. Ensembles of solution conformations for the *trans* forms of these 17-residue disulfide-bridged peptides have been generated using a simulated annealing procedure in conjunction with distance and torsion angle restraints derived from NMR data. Comparison of the NMR-derived solution structures of the PAO and KB7 peptides with that previously determined (McInnes *et al.*, 1993) and herein refined for the PAK peptide reveals a common structural motif. All three peptide structures contain a type I β-turn in the conserved sequence Asp^{134}-X-X-Phe^{137} and a type II β-turn in the conserved sequence Pro^{139}-X-Gly-Cys^{142}. However, the overall folds of the three peptides differ as well as the disposition of the side chains comprising the hydrophobic pockets. The similarities and differences between the structures of the three strains which bind to a common cell surface receptor are discussed in light of their contributions to synthetic vaccine design.

Pseudomonas aeruginosa is a Gram-negative rod-shaped bacterium which causes infections resulting in opportunistic respiratory disease in cancer, cystic fibrosis, and intensive care patients (Rivera & Nicotra, 1982; Pier, 1985; Todd *et al.*, 1989; Sajjan *et al.*, 1991; Irvin *et al.*, 1993). The initial step in the pathogenicity of *P. aeruginosa* is believed to be adherence to the host cell via polar pili on the bacterial surface (Pier, 1985; Paranchych *et al.*, 1986; Irvin, 1993). The pili are proteinaceous filaments composed of a homologous polymer of pilin protein and are assembled into a helical array to form a hollow tube (Irvin, 1993). The pilin monomer has been shown to contain the binding domain of *P. aeruginosa* to host epithelial cells (Ramphal *et al.*, 1984; Paranchych *et al.*, 1986; Doig, 1987, 1988, 1990; Irvin *et al.*, 1989). The pilin can be roughly divided into three regions: a conserved N-terminal region, a hypervariable central region, and a semiconserved C-terminal region. The C-terminal region of the pilin monomer contains the epithelial cell binding domain (Paranchych *et al.*, 1986; Irvin *et al.*, 1989; Lee *et al.*, 1989), and recently it has been shown that binding of the pili is a tip-associated event involving the C-terminal region of the structural pilin subunit (Lee *et al.*, 1994). The seven different strains of *P. aeruginosa* share a common glycosphingolipid cell surface receptor (Ramphal *et al.*, 1984, 1991) where the minimal structural element is a disaccharide shown to specifically bind strains PAK and PAO (Lee *et al.*, 1994; Sheth *et al.*, 1994) despite a limited degree of homology between their C-terminal domains (Pasloske *et al.*, 1988; Paranchych *et al.*, 1990) (a disulfide loop of 17 residues and a conserved proline; Figure 1).

In counteracting *P. aeruginosa* infections, an anti-adhesin vaccine has been proposed. Antibodies specific for the pilus C-terminal region can be raised using synthetic peptides and used to counteract infection by blocking bacterial attachment (Lee *et al.*, 1990). Since *P. aeruginosa* exists as seven different strains, production of cross-reactive antibodies effective against all strains would be most desirable. It is possible to envisage such a cross-reactive antibody since all strains bind to the same receptor (Ramphal *et al.*, 1984, 1991; Krivan *et al.*, 1988a,b; Baker *et al.*, 1990).

The development of vaccines for the production of cross-reactive antibodies requires an understanding of the molecular nature of the antibody−antigen recognition process and an understanding of the factors which specify strain recognition and cross-reactivity between strains. Recent studies on the structure of antigens in their antibody bound and free forms have revealed a great deal about the nature of antibody−antigen recognition. The identification of secondary structure elements in free antigenic peptides suggests that antibodies are produced in response to the recognition of regions of peptides and proteins which contain exposed structures such as β-turns (Dyson *et al.*, 1985, 1988a,b; Chandrasekhar *et al.*, 1991; Zvi *et al.*, 1992; Blumenstein *et al.*, 1992). Indeed, a large number of antigenic peptides have been shown to adopt turn conformations, indicating that these may constitute a structural motif for antibody recognition. The criteria of stable conformations and surface-accessible secondary structure (Kuntz, 1972; Scherf *et al.*, 1992) are met with turn regions of immunogenic peptides and proteins. These criteria are likely necessary in order for binding of an immunogen to a B-cell receptor to elicit an immune response (De Lorimier *et al.*, 1994).

[†] This work was funded by the Medical Research Council of Canada and the Protein Engineering Network of Centres of Excellence, which is funded by the Government of Canada.

[‡] Coordinates have been deposited in the Brookhaven Protein Data Bank under the file names 1KB8, 1NIM, and 1PAO.

* Author to whom correspondence should be addressed [Tel: (403) 492-6540. Fax: (403) 492-1473. Email: bds@polaris.biochem.ualberta.ca].

[⊗] Abstract published in *Advance ACS Abstracts,* November 15, 1995.

0006-2960/95/0434-16255$09.00/0

In the current study, the NMR solution structures for the C-terminal receptor binding peptides from the pilin strains PAO and KB7 have been determined, and a comparison has been made to a refined structure of the PAK C-terminal peptide previously studied by McInnes *et al.* (1993). A knowledge of the three-dimensional solution structures of the PAO, KB7, and PAK receptor binding regions should allow determination of a structural motif for antibody and receptor recognition, as well as a greater comprehension of the factors contributing to immunogenicity. This structural information should facilitate the development of a broad spectrum vaccine against multiple strains involved in *P. aeruginosa* infections.

EXPERIMENTAL PROCEDURES

Peptide Synthesis. *P. aeruginosa* strain PAO pilin residues 128−144, Ac-ACKSTQDPMFTPKGCDN-OH, and KB7 pilin residues 128−144, Ac-SCATTVDAKFRPNGCTD-OH, were synthesized and purified by solid-phase peptide synthesis and purified by reversed-phase HPLC as previously reported (Wong *et al.*, 1992, 1995). Amino acid analysis was performed on a Beckman Model 6300 amino acid analyzer (Beckman, San Ramon, CA). Mass analysis of the peptides was performed on a Fisons VG Quattro triple quadrupole mass spectrometer (Manchester, England) fitted with an electrospray ionization source operating in the positive ion mode. Ten microliter injections of the peptide samples (usually in aqueous acetonitrile containing 0.05% trifluoroacetic acid at an approximate concentration of 50 pmol/μL) were made into a carrier solution composed of 1:1 (v/v) water−acetonitrile containing 0.05% trifluoroacetic acid at a rate of 10 μL/min into the electrospray source. The quadrupoles were scanned from 600 to 1400 mass over charge ratios at 10 s/scan. Data were acquired in the MCA mode with typically 10−15 scans being summed to produce a spectrum.

As with PAK, these peptides were studied in their oxidized forms with the disulfide bridge between residues 129 and 142 (Figure 1). The intramolecular disulfide bridge was obtained by air oxidation of the appropriate reduced peptides. Typically, the reduced peptides were dissolved in 100 mM NH_4HCO_3, pH 8.0, at a total concentration of approximately 0.2 mg/mL. Then the solution was magnetically stirred for 24 h while exposed to air. Verification of the intra-disulfide bridge was determined by both reversed-phase HPLC retention change and electrospray mass spectroscopy as described above.

NMR Sample Preparation. Samples were prepared by dissolving PAO 128−144 and KB7 128−144 in 500 μL of 90% H_2O/10% D_2O containing 100 mM KCl and 20 mM NaOAc to a concentration of 5 mM. 2,2-Dimethyl-2-sila-5-pentanesulfonate (DSS) was added as an internal chemical shift reference and the pH subsequently adjusted to 5.0 using NaOD and DCl solutions.

NMR Spectroscopy. ^{1}H NMR spectra for PAO 128−144 and KB7 128−144 were acquired at 500 and 600 MHz, respectively, using Varian Unity 500 and 600 spectrometers. These included one- and two-dimensional experiments collected at 5.0, 10.0, 15.0, 20.0, and 25 °C using presaturation for 2.5 s at a power level of 28 dB (γB_2 = 50 Hz) through which suppression of the water resonance was attained. The hypercomplex method was used for acquisition of two-dimensional experiments (States *et al.*, 1982) which typically incorporated 32 transients for each of 300 increments with 2048 data points along t_2 and included DQF-COSY (Piatini *et al.*, 1982; Rance *et al.*, 1983), TOCSY (Bax & Davis, 1985), NOESY (Jeener *et al.*, 1979; Macura & Ernst, 1980), and SCUBA-NOESY (Brown *et al.*, 1988) spectra. Water suppression for each of these two-dimensional experiments was achieved using presaturation for 2.0 s at a power level of 28 dB. The TOCSY employed a spin-lock field of 7.12 kHz. Distance restraints were obtained for PAO 128−144 using NOESY experiments performed at 500 MHz, 5.0 °C, using a spectral width of 6000 Hz and a mixing time of 300 ms. Distance restraints were obtained for KB7 128−144 using SCUBA-NOESY experiments performed at 600 MHz, 5.0 °C, using a spectral width of 7000 Hz and a mixing time of 175 ms. The Fourier transformation of the spectra utilized sine-bell processing with a phase shift of 90° and zero filling to 4K × 4K. Proton resonances were assigned (Table 1) using the sequential assignment technique (Wüthrich, 1986).

Data Analysis and 3-D Structure Calculation. Interproton distance restraints for PAO 128−144 and KB7 128−144 were generated through integration of cross-peaks from the NOESY and SCUBA-NOESY spectra acquired at 5.0 °C. The integral volumes obtained were converted to distance restraints using a reference distance of 2.55 Å for the β to δ interproton of Phe^{137}.[1] The restraint file was then generated from these volumes using a program written by R. Boyko and F. Sönnichsen (University of Alberta). The distance classifications generated were strong (van der Waals radii $\leq r_{ij} \leq$ 2.7 Å), medium (1.8 Å $\leq r_{ij} \leq$ 3.3 Å), and weak (2.3 Å $\leq r_{ij} \leq$ 5.0 Å). The resulting restraint file was then edited such that distances associated with ambiguous assignments were removed and distances arising from certain but overlapping NOEs were classified as weak and with extended upper boundaries (van der Waals radii $\leq r_{ij} \leq$ 5.0 Å).

Temperature coefficients ($-\Delta\delta/\Delta T$, ppb) were obtained using data from NOESY and SCUBA-NOESY spectra acquired at 5.0, 10.0, 15.0, and 20.0, and 25.0 °C and were calculated from plots of chemical shift versus temperature which were linear for all amide protons in PAO 128−144 and KB7 128−144 (Table 2). Four generic distance restraints were used, corresponding to the hydrogen bonds between the Asp^{134} carbonyl and Phe^{137} NH and the Pro^{139} carbonyl and Cys^{142} NH in each peptide (Asp^{134} O−Phe^{137} NH ≤ 2.5 Å; Asp^{134} O−Phe^{137} N ≤ 3.0 Å; Pro^{139} O−Cys^{142} NH ≤ 2.5 Å; Pro^{139} O−Cys^{142} N ≤ 3.0 Å).

$^3J_{NH\alpha CH}$ coupling constants were obtained from 2K × 2K ($f_2 \times f_1$) DQF-COSY spectra acquired at 5.0 °C. The spectra were zero-filled to 16K in the f_2 dimension and processed using 90° shifted sine-bell weighting in the f_1 dimension and no weighting in the f_2 dimension. Traces for resolved cross-peaks were taken in ω_2 and then curve-fitted using a program written by R. Boyko and F. Sönnichsen (University of Alberta) which utilizes an iterative fitting procedure. The $^3J_{NH\alpha CH}$ coupling constants were converted into ϕ restraints using the Karplus equation (Karplus, 1963) with the following constants: $A = 6.7$, $B = -1.3$, and $C = 1.5$. Only coupling constants ≥8 Hz and ≤6 Hz were used in structure calculations. These included $^3J_{NH\alpha CH}$ = 8.9, 5.5, and 8.0 Hz

[1] The β to δ interproton distance in phenylalanine residues varies within 2.55 ± 0.15 Å as the torsion angle χ_i^2 between the Cβ and Cγ carbons is rotated around 360° (Billeter *et al.*, 1982).

for T^{130}, K^{140}, and C^{142}, respectively, in the PAK peptide; $^3J_{NH\alpha CH} = 5.0$, 5.7, 8.0, and 8.0, Hz for A^{128}, K^{140}, C^{142}, and N^{144}, respectively, in the PAO peptide; and $^3J_{NH\alpha CH} = 4.5$, 8.0 and 8.6 Hz for A^{135}, F^{137}, and T^{143}, respectively, in the KB7 peptide. Thirty degrees was subtracted from the lower boundaries and added to the upper boundaries of these ϕ restraints ($\phi \pm 30°$) in order to account for inacuracies associated with the significant flexibility of these peptides.

Stereospecific assignments and torsion angle ψ restraints (for the PAK peptide only) were generated using the Stereosearch program (Nilges *et al.*, 1990), which requires a $^3J_{NH\alpha CH}$ coupling constant and sequential NOE information as input. Stereosearch uses an error margin of ±20° on its calculated ψ restraint values ($\psi \pm 20°$). This error margin was extended to ±40° ($\psi \pm 40°$) again in order to account for the significant flexibility of these peptides (as opposed to protein structures for which Stereosearch was originally designed). Using the Stereosearch program, stereospecific assignments (*R*, *S*) (Cahn *et al.*, 1956) of β and δ protons were obtained for residues Cys^{129}, Phe^{137}, and Pro^{139} in the PAK peptide, Cys^{129}, Pro^{135}, and Pro^{139} in the PAO peptide, and Cys^{129}, Phe^{137}, and Pro^{139} in the KB7 peptide. These assignments are given in Table 1. Additional stereospecific assignments were made as the structure calculations were performed (see below). A summary of the constraints used for structure generation of PAK 128−144, PAO 128−144, and KB7 128−144 is given in Table 3.

Structural calculations were performed as described previously (McInnes *et al.*, 1993) using Biosym software (San Diego, CA) and a Silicon Graphics Iris Crimson hardware platform. Calculations were performed utilizing a simulated annealing (SA) protocol adapted from that of Nilges *et al.* (1988) which employs the CVFF force field. This searches for the global minimum of a target function which is comprised of the standard energy terms of the CVFF force field for bonded interactions and a simple quartic nonbonded potential with van der Waals radii. The distance information was included using a skewed biharmonic potential which was equal for all restraints. All peptide bonds were forced to *trans*[2] geometry during the calculations. Charge interactions and cross terms were not included in the calculations. A cutoff distance of 5 Å for nonbond interactions was used.

The calculations consisted of 14 stages including an initial energy minimization of randomly distributed atoms (100 steps steepest descent and 2000 steps conjugate gradient), 55 ps of molecular dynamics in 3 stages at 1000 K, during which the NOE force constants were scaled from 0.00001 to 20 kcal, 10 ps of molecular dynamics during cooling to 300 K in 5 stages, and a final full-energy minimization in 4 stages (100 steps steepest descent, 2000 steps conjugate gradient, 100 steps steepest descent, and 15 000 steps conjugate gradient).

Calculation of the PAO and KB7 structures and refinement of the previously determined PAK structure were performed using a program, PEPFLEX-II (Wang *et al.*, 1995), which combines the restrained SA protocol outlined above with an ensemble full-relaxation matrix approach and an iterative NOE restraint modification procedure. The PEPFLEX-II program addresses the problem of solving solution structures for flexible peptides which can exist in solution as a large ensemble of interchangeable conformations. Since this interconversion is fast on the NMR time scale, structural information obtained is the "average" of these multiple conformations and can lead to a meaningless "averaged" structure. PEPFLEX-II allows the flexible peptide to sample a wider conformational space. A series of iterative NOE restraint modifications lead to a final distance restraint file, which is obtained when the NOEs calculated and averaged from a final family of structures best agree with the original experimental NOEs. By definition, the final family of structures is obtained when a minimized total RMS deviation, calculated as the squared sum of the differences between averaged calculated and experimental NOEs, is obtained.

Iterative refinement of the peptide structures with the PEPFLEX-II program allowed additional stereospecific assignments to be made of protons which could not be unambiguously assigned from the Stereosearch program. Stereospecific assignments were possible where local backbone and side-chain RMSDs in the family of peptide structures were sufficiently low (<1.0) to observe a well-defined stereochemistry around the Cα or Cβ carbon of selected residues (generally a result of longer range NOEs involving the β protons of the residue). For example, iterative refinement produced well-defined turn regions involving residues Asp^{134}−Phe^{137} and Pro^{139}−Cys^{142} in all three peptide structures. This allowed the assignment of stereospecific NOEs involving the α protons of Gly^{141} and the β protons of Asp^{134} and Cys^{142}. Stereospecific assignments were thus obtained for the α and β protons of residues Asp^{134} and Gly^{141} in the PAK peptide, Asp^{134}, Gly^{141}, and Cys^{142} in the PAO peptide, and Gly^{141} in the KB7 peptide (see Table 1).

A total of 7, 16, and 9 rounds of SA/PEPFLEX-II was performed on the PAK, PAO, and KB7 peptides, respectively, to obtain a modified restraint file where no violations of >0.3 Å were observed in the ensemble family of structures group for less than 10% of the total number of distance restraints. A total of 35 consecutive SA runs was then performed from the final distance restraint file to generate 35 structures for each peptide, and an average structure was calculated and energy minimized using steepest descents and conjugate gradients. The average energy-minimized structure was then analyzed using the programs VADAR (Wishart *et al.*, 1994) and PROCHECK (Laskowski *et al.*, 1993) to assess the quality of the structure.

RESULTS

Resonance Assignments and Chemical Shifts. The amino acid sequences of *P. aeruginosa* strains PAK, PAO, and KB7 pilin C-terminal residues 128−144 are aligned in Figure 1, and although this region displays limited homology, there are residues which are conserved across the three strains (Cys^{129}, Asp^{134}, Phe^{137}, Pro^{139}, Gly^{141}, and Cys^{142}). These conserved residues may confer a conserved structural motif to the C-terminal region of the pilin protein since all three strains bind with this region to a common glycosphingolipid cell surface receptor (Ramphal *et al.*, 1984, 1991; Krivan *et*

[2] Restraint of all X-Pro peptide bonds (Ile^{138}−Pro^{139} in PAK, Asp^{134}−Pro^{135} and Thr^{138}−Pro^{139} in PAO, and Arg^{138}−Pro^{139} in KB7) to *trans* geometry during the calculations was considered reasonable given that the pattern of dominant X-Pro NOE connectivities observed in the NOESY spectra of the peptides confirmed a *trans* configuration (see Results section). In addition, earlier structure calculations of the pilin peptides leaving the X-Pro peptide bonds unrestrained resulted in *trans* geometries around these bonds.

Strain	128	129	130	131	132	133	134	135	136	137	138	139	140	141	142	143	144
PAK	K	**C**	T	**S**	D	Q	**D**	E	Q	**F**	I	**P**	K	**G**	**C**	**S**	K
KB7	S	**C**	A	T	T	V	**D**	A	K	**F**	R	**P**	N	**G**	**C**	T	D
PAO	A	**C**	K	**S**	T	Q	**D**	P	M	**F**	T	**P**	K	**G**	**C**	D	N
CD4	T	**C**	T	**S**	T	Q	**E**	E	M	F	I	P	K	G	**C**	N	K
K122-4	A	**C**	T	**S**	N	A	**D**	N	K	Y	L	P	K	T	**C**	Q	T

FIGURE 1: Primary structure of the C-terminal region (residues 128−144) of five strains of *P. aeruginosa*. Residues in boldface are those conserved in the PAK, PAO, and KB7 strains. Residues which are conserved in all strains are in the shaded box, while semiconserved residues are in the white box.

al., 1988a,b; Baker *et al.*, 1990) and compete for a common receptor on the epithelial cell surface (Doig *et al.*, 1990; Lee *et al.*, 1994).

The ^{1}H NMR assignments for the PAK, PAO, and KB7 peptides at pH 5.0, 5.0 °C, are presented in Table 1. A superficial inspection of the table shows that some conserved residues, such as C^{142}, have similar chemical shifts across the strains (C^{142} αCH shifts are 4.78 ppm in PAK, 4.75 ppm in PAO, and 4.80 ppm in KB7), whereas other conserved residues, such as D^{134}, have substantially different chemical shifts across the strains (D^{134} αCH shifts are 4.60 ppm in PAK, 4.84 ppm in PAO, and 4.55 ppm in KB7).

The chemical shift similarities and differences of residues across the three strains are easier to assess when the differences between backbone proton chemical shifts and their random coil values are calculated. Deviations from random-coil values of αCH and NH protons are indicative of secondary structure in that all 20 naturally occurring amino acids experience a mean α-proton shift of −0.39 ppm (upfield from the random-coil value) when placed in a helical configuration, whereas a mean α-proton shift of +0.37 ppm is experienced when the residue is placed in an extended configuration (Wishart *et al.*, 1991). Figure 2A presents a plot of $\Delta\delta_{\alpha CHobs-coil}$ versus residue position for the PAK, PAO, and KB7 peptides where no $\Delta\delta_{\alpha CHobs-coil}$ values greater than ±0.3 ppm for any of the residues in the three peptides can be seen. This suggests that the three peptides possess a certain degree of conformational flexibility since there are no strongly delineated helical or extended regions defined from the αCH chemical shift values. This conformational flexibility is also suggested in Figure 2B, which presents a plot of $^3J_{NH\alpha CH}$ coupling constant versus residue position for the three peptides. The majority of $^3J_{NH\alpha CH}$ coupling constant values are greater than 6 Hz and less than 8 Hz, indicating that the peptides are quite flexible, possibly undergoing a conformational equilibrium between helical and extended dihedral space.

Further evidence for peptide flexibility comes from calculation of the ratio of the $d_{\alpha N}(i,i)$ and $d_{\alpha N}(i-1,i)$ NOEs, $d_{N\alpha}/d_{\alpha N}$. The magnitude of this ratio is dependent mainly on the ψ dihedral angle of residue $(i-1)$; thus for $d_{N\alpha}/d_{\alpha N} > 1.1$, $\psi(i-1)$ is in α-helical conformational space, whereas for $d_{N\alpha}/d_{\alpha N} < 0.83$, $\psi(i-1)$ is in β-strand conformational space.[3] Measurement of $d_{N\alpha}/d_{\alpha N}$ ratios for all possible residues in the PAK, PAO, and KB7 peptides yields values $0.83 < d_{N\alpha}/d_{\alpha N} < 1.1$, suggestive of no rigidly defined regions of α-helix or β-strand.

[3] The NH(i)−αCH($i-1$) distance corresponding to $d_{\alpha N}(i,i)$ is covalently fixed in the 2.7−3.1 Å range for the α-helix and β-strand, whereas the NH(i)−αCH($i-1$) distance corresponding to $d_{\alpha N}(i-1,i)$ is 3.4−3.6 Å for the α-helix and 2.2−3.1 Å for the β-strand. Consequently, the $d_{N\alpha}/d_{\alpha N}$ ratio is >1.1 for the α-helix and <0.83 for the β-strand (Gagné *et al.*, 1994).

Table 1: ^{1}H NMR Assignments of PAK, PAO, and KB7 128−144 *Trans* Isoforms

residue	NH	α-CH	β-H	γ-H	δ-H and others
			(A) PAK 128−144 (pH 5.0, 5 °C)		
K^{128}	8.44	4.35	1.84, 2.05	1.47	1.77, ε 2.98
C^{129}	8.82	4.81	$2.99^{R,a}$ 3.32^{S}		
T^{130}	8.29	4.48	4.32	1.22	
S^{131}	8.52	4.53	3.89		
D^{132}	8.52	4.61	2.72		
Q^{133}	8.33	4.29	2.00, 2.15	2.35	
D^{134}	8.42	4.60	2.73^{R}, 2.82^{S}		
E^{135}	8.42	4.20	2.01, 2.12	2.34	
Q^{136}	8.53	4.16	1.90	2.10	
F^{137}	8.07	4.64	3.03^{R}, 3.18^{S}		δ 7.23, ε 7.34, ζ 7.29
I^{138}	8.07	4.38	1.82	1.14, 1.53	0.84, 0.89
P^{139}		4.36	1.94^{R}, 2.36^{S}	1.99, 2.07	3.63^{S}, 3.87^{R}
K^{140}	8.54	4.23	1.84	1.47, 1.53	1.70, ε 3.00
G^{141}	8.68	3.91^{R}, 4.05^{S}			
C^{142}	8.15	4.78	3.00, 3.22		
S^{143}	8.53	4.52	3.89		
K^{144}	8.22	4.17	1.84	1.43	1.74, ε 3.00
			(B) PAO 128−144 (pH 5.0, 5 °C)		
A^{128}	8.44	4.27	1.35		
C^{129}	8.64	4.64	3.01^{R}, 3.21^{S}		
K^{130}	8.48	4.38	1.77, 1.91	1.43	1.64, ε 2.96
S^{131}	8.44	4.46	3.85, 3.93		
T^{132}	8.22	4.06	4.18	1.07	
Q^{133}	8.31	4.27	1.92, 2.13	2.32	
D^{134}	8.22	4.84	2.61^{R}, 2.87^{S}		
P^{135}		4.42	2.03^{R}, 2.33^{S}	1.96	3.67^{S}, 3.87^{R}
M^{136}	8.70	4.39	1.89	2.48	2.31
F^{137}	7.95	4.56	3.10		δ 7.18, ε 7.31, ζ 7.27
T^{138}	7.91	4.48	4.05	1.16	
P^{139}		4.29	2.00^{R}, 2.32^{S}	1.96	3.67^{S}, 3.87^{R}
K^{140}	8.36	4.23	1.77	1.44	1.66, ε 2.96
G^{141}	8.51	3.86^{R}, 4.00^{S}			
C^{142}	8.19	4.75	2.93^{S}, 3.23^{R}		
D^{143}	8.59	4.65	2.59, 2.75		
N^{144}	8.06	4.43	2.64, 2.74		
			(C) KB7 128−144 (pH 5.0, 5 °C)		
S^{128}	8.46	4.52	3.88, 3.94		
C^{129}	8.92	4.70	2.98^{R}, 3.28^{S}		
A^{130}	8.44	4.37	1.43		
T^{131}	8.19	4.44	4.33	1.22	
T^{132}	7.99	4.43	4.34	1.21	
V^{133}	8.19	4.09	2.12	0.97	
D^{134}	8.47	4.55	2.75		
A^{135}	8.26	4.11	1.42		
K^{136}	8.39	4.10	1.63	1.15	1.57, ε 2.91
F^{137}	8.01	4.67	2.99^{R}, 3.25^{S}		δ 7.25, ε 7.36, ζ 7.30
R^{138}	8.07	4.63	1.72, 1.81	1.65	3.19
P^{139}		4.38	2.01^{R}, 2.35^{S}	1.92	3.61^{S}, 3.71^{R}
N^{140}	8.69	4.65	2.82		
G^{141}	8.49	3.90^{R}, 4.05^{S}			
C^{142}	8.22	4.80	3.00, 3.25		
T^{143}	8.49	4.45	4.32	1.19	
D^{144}	8.20	4.44	2.65, 2.75		

[a] The R, S stereochemistry of the β protons is according to the Cahn−Ingold−Prelog convention (Cahn et al., 1956).

Regardless of the inherent flexibility of the PAK, PAO, and KB7 peptides, a close inspection of Figures 2 does reveal

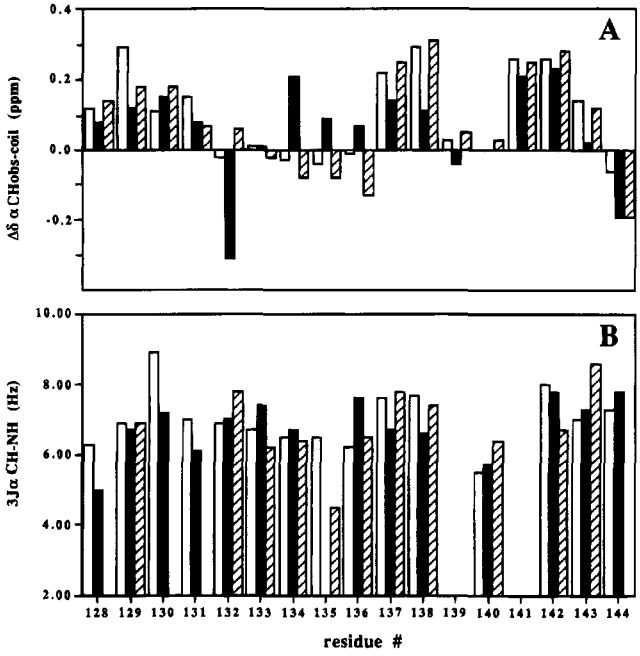

FIGURE 2: Plots of (A) the difference in NMR chemical shift (observed − random coil) for the αCH proton $\Delta\delta_{\alpha CHobs-coil}$ and (B) the NHαCH vicinal NMR coupling constant $^3J_{NH\alpha CH}$ versus sequence for PAK 128−144 (white box), PAO 128−144 (black box), and KB7 128−144 (cross-hatched box) measured from ^1H NMR data taken at pH 5, 5.0 °C.

Table 2: Temperature Coefficient Values for PAK, PAO, and KB7 128−144 *Trans* Isoforms

	$-\Delta\delta/\Delta T \times 1000$[a]		
residue	PAK	PAO	KB7
128	7.0	6.8	7.5
129[b]	7.0	7.3	9.5
130	7.0	6.8	5.5
131	7.0	6.8	6.5
132	5.0	6.2	4.0
133	5.5	3.4	6.5
134	6.5	6.9	8.5
135	5.0		7.0
136	5.5	6.5	6.5
137	3.5	2.5	5.0
138	7.0	3.7	6.5
139			
140	8.0	6.2	9.0
141	7.5	6.2	7.5
142	3.0	2.3	3.0
143	7.0	4.6	8.0
144	8.5	6.0	7.5

[a] Uncertainty in the temperature coefficient values is ±0.5 ppb/K. [b] Boldface indicates residues conserved in PAK, PAO, and KB7.

some common structural features. Residues 129, 130, 131, 137, 138, 141, and 142 show upfield shifts of 0.1−0.3 ppm for the αCH protons in all three peptides (Figure 2A), suggestive of an extended configuration. The $^3J_{NH\alpha CH}$ coupling constants for these same residues (except for 141) are all greater than 6 Hz[4] (Figure 2B), consistent with a ϕ angle in extended or β-strand dihedral space ($\phi < -70°$). Structural differences between the peptides are seen for residues 132 and 134, which show significant differences in chemical shifts across the three strains (Figure 2A).

[4] $^3J_{NH\alpha CH}$ values ≥8 Hz are observed for T^{130} and C^{142} in the PAK peptide, C^{142} in the PAO peptide, and F^{137} in the KB7 peptide.

Temperature Coefficients. The temperature dependence of the amide proton chemical shift is an indication of possible intramolecular hydrogen bonding. For a random-coil peptide in water, the temperature coefficients of the amide proton resonances are expected to be $6 \leq -\Delta\delta/\Delta T \leq 10$ ppb, whereas for amides protected from exchange with the solvent these values are expected to decrease to $-\Delta\delta/\Delta T \leq 5$ ppb (Rose *et al.*, 1985). The temperature coefficients for the amide backbone protons of the PAK, PAO, and KB7 peptides are shown in Table 2. The decreased temperature coefficients of the amides of Phe^{137} and Cys^{142} in the PAO and KB7 peptides suggest hydrogen bonding to these residues. On the basis of these temperature coefficients and NOE patterns (discussed below), putative hydrogen bonds were identified as Asp^{134} CO−Phe^{137} NH and Pro^{139} CO−C^{142} NH, in agreement with those identified in the PAK pilin peptide (McInnes *et al.*, 1994).

Secondary Structure. The NOEs diagnostic of β-turns include $d_{\alpha N}(2,3)$, $d_{\alpha N}(3,4)$, $d_{\alpha N}(2,4)$, $d_{NN}(2,3)$, and $d_{NN}(3,4)$ cross-peaks (Wüthrich *et al.*, 1984; Wagner *et al.*, 1986), where the numbering indicates the position in the turn. The NOEs required for positive identification of a β-turn are a weak $d_{\alpha N}(2,4)$ cross-peak, corresponding to a distance of 3.6 Å in the type I turn and 3.3 Å in the type II turn, and a strong $d_{NN}(3,4)$ cross-peak, corresponding to a distance of 2.4 Å in both types of turns (Wüthrich *et al.*, 1984). Type I and type II turns may be distinguished by the relative strengths of the $d_{\alpha N}(2,3)$ and the $d_{NN}(2,3)$ cross-peaks. The type I turn displays a medium $d_{\alpha N}(2,3)$ cross-peak and a strong $d_{NN}(2,3)$ cross-peak, corresponding to distances of 3.4 and 2.6 Å, respectively, whereas the type II turn displays a strong $d_{\alpha N}(2,3)$ cross-peak and a weak $d_{NN}(2,3)$ cross-peak, where the corresponding distances are 2.2 and 4.5 Å.

Figure 3 shows the d_{NN}, $d_{\alpha N}$, and $d_{\beta N}$ regions of the NOESY spectra of the oxidized PAK (Figure 3A), PAO (Figure 3B), and KB7 (Figure 3C) peptides at pH 5.0, 5.0 °C. Under these conditions the spectra exhibit similar NOE connectivities. All three peptides display strong $d_{NN}(3,4)$ cross-peaks between X^{136} and Phe^{137} and between Gly^{141} and Cys^{142}, and weak $d_{\alpha N}(2,4)$ cross-peaks are observed between X^{140} and Cys^{142} in the PAK and PAO spectra (Figure 3A,B). The $d_{\alpha N}(2,4)$ cross-peak between Asn^{140} and Cys^{142} in the KB7 spectra can be observed at lower thresholds. A weak $d_{\alpha N}(2,4)$ cross-peak is observed between Glu^{135} and Phe^{137} in the PAK spectrum as a shoulder on the strong Gln^{136}−Phe^{137} $d_{\alpha N}(3,4)$ cross-peak (Figure 3A). $d_{\alpha N}(2,4)$ cross-peaks between X^{135} and Phe^{137} in the PAO and KB7 spectra are overlapped with the strong X^{136}−Phe^{137} $d_{\alpha N}(3,4)$ cross-peaks (Figure 3B,C). The $d_{NN}(3,4)$ and $d_{\alpha N}(2,4)$ NOEs described above are diagnostic of two β-turns in the regions Asp^{134}-X-X-Phe^{137} and Pro^{139}-X-Gly-Cys^{142}. Other NOEs which suggest the presence of β-turns in these regions are those observed in the $d_{\beta N}$ region of the PAK and PAO spectra (Figure 3A,B) between the β protons of Asp^{134} and X^{135} and the backbone NH of Phe^{137} and between the β protons of Pro^{139} and X^{140} and the backbone NH of Cys^{142} (the Pro^{139}−Cys^{142} $d_{\beta N}$ NOE is observed at lower thresholds in the PAO spectrum in Figure 3B).

Additional evidence for the turns is afforded by the small temperature coefficients of the Phe^{137} and Cys^{142} backbone amides for all three peptides (see Table 2), a likely consequence of its involvement in the (1,4) hydrogen bond present between the carbonyl oxygen of the first residue in

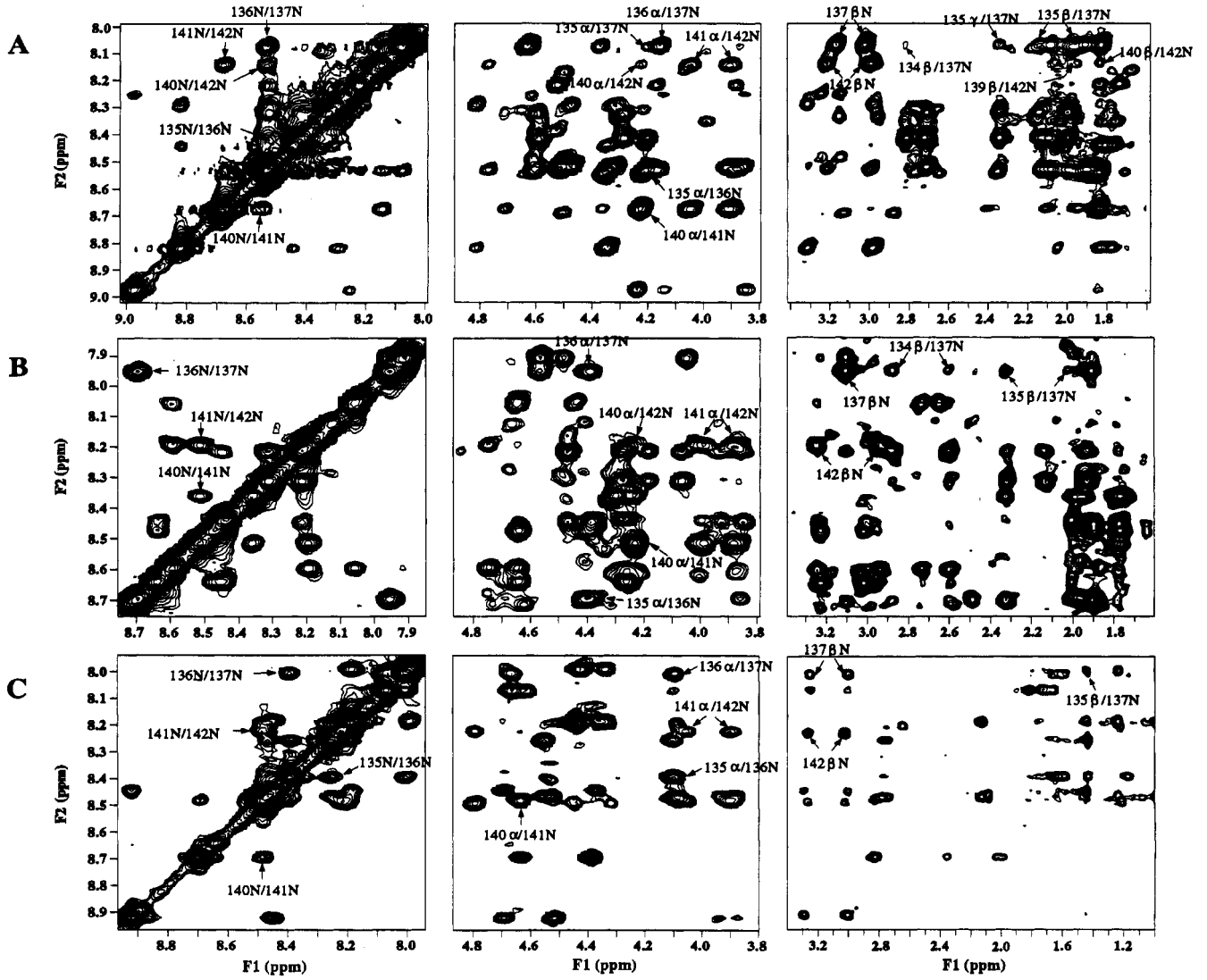

FIGURE 3: d_{NN}, $d_{\alpha N}$, and $d_{\beta N}$ regions of the (A) 600 MHz NOESY spectrum of oxidized 5 mM PAK 128−144, (B) 500 MHz NOESY spectrum of oxidized 5 mM PAO 128−144, and (C) 600 MHz SCUBA-NOESY spectrum of oxidized 5 mM KB7 128−144. All peptides are in 90% H_2O/10% D_2O, pH 5, 20 mM NaOAc, and 100 mM KCl at 5.0 °C. NOEs identifying observed β-turns are labeled.

the turn and the amide hydrogen of the last residue in the turn (Asp[134] CO−Phe[137] NH and Pro[139] CO−C[142] NH) (Rose *et al.*, 1985). In addition, the $^3J_{NH\alpha CH}$ coupling constants for residues 135 and 140 in position 2 of the putative turns are 6.4 and 5.5 Hz for Glu[135] and Lys[140] in the PAK peptide, 5.7 Hz for Lys[140] in the PAO peptide ($^3J_{NH\alpha CH}$ for Pro[135] in the PAO peptide cannot be measured), and 4.5 and 6.3 Hz for Ala[135] and Asn[140] in the KB7 peptide (see Figure 2B). These coupling constants are all equal to or less than 6.4 Hz and consistent with a ϕ angle greater than −70°, and therefore consistent with $\phi_2 = -60°$ for most turns (Richardson, 1981).

The presence of strong $d_{\alpha N}(2,3)$ and weak $d_{NN}(2,3)$ cross-peaks between X[140] and Gly[141] for all three peptides (see Figure 3) suggests a predominant concensus configuration of type II for the turn spanning Pro[139]-X-Gly-Cys[142] (Chandrasekhar *et al.*, 1991). The configuration of the turn spanning Asp[134]-X-X-Phe[137] is somewhat less obvious on the basis of the relative intensities of the $d_{\alpha N}(2,3)$ and $d_{NN}(2,3)$ cross-peaks. The PAK spectrum (Figure 3A) displays a strong $d_{NN}(2,3)$ cross-peak between Glu[135] and Gln[136], although it is not possible to determine the intensity of the $d_{\alpha N}(2,3)$ cross-peak since it is overlapped with another. The PAO spectrum (Figure 3B) displays a moderately strong $d_{\alpha N}$-(2,3) cross-peak between Pro[135] and Met[136] but no $d_{NN}(2,3)$ cross-peak since Pro[135] contains no backbone amide. In the KB7 spectrum (Figure 3C), both $d_{\alpha N}(2,3)$ and $d_{NN}(2,3)$ cross-peaks between Ala[135] and Lys[136] are moderately strong. Although the relative intensities of these NOEs do not lead to a concensus of configuration across the first turn, the presence of the population of the type I turn is suggested by moderately strong $d_{\beta N}(2,4)$ connectivities between X[135] and Phe[137] for all three peptides since this distance can approach as closely as 2.9 Å in a type I turn but only as close as 3.6 Å in a type II turn. The $d_{\beta N}(2,4)$ connectivity between X[140] and Cys[142] is absent in the PAO and KB7 spectra (Figures 3B,C) and is comparatively very weak in the PAK spectrum (Figure 3A), consistent with a configuration of type II for the second turn in all three peptides.

Cis versus Trans Isomers. The oxidized PAK peptide has been found to exist as two distinct conformations in solution which have been demonstrated to arise as a result of isomerization of the Ile[138]−Pro[139] peptide bond (McInnes *et al.*, 1994). The *cis* isomer was shown to exist in the oxidized form of the peptide to a significant degree (20%) in water at 5 °C (McInnes *et al.*, 1993). The PAO and KB7 peptide sequences both contain the conserved Pro[139] residue, with

an additional proline, Pro^{135}, in the PAO sequence. Any of these prolines could provide a site for isomerization leading to *cis* and *trans* isomers around $Asp^{134}-Pro^{135}$ and $Thr^{138}-Pro^{139}$ in the PAO peptide and $Arg^{138}-Pro^{139}$ in the KB7 peptide. Thus, there could potentially be two KB7 isomers and four PAO isomers in solution. However, unlike the oxidized PAK peptide for which the *cis* isomer is present to a significant degree at 5 °C, no *cis* isomers can be observed for either the oxidized PAO or the oxidized KB7 peptide in solution at the same temperature. The one-dimensional spectra of the PAO and KB7 peptides show no clear additional resonances attributable to the presence of well-populated major and minor species. Only exceedingly weak resonances barely distinguishable above the baseline noise can be attributed to minor species which must be present to less than 5% of the total population of peptide in solution. The pattern of NOE connectivities connecting the major resonances confirms that the conformations are *trans* around the X−Pro bonds. Strong $d_{\alpha\delta}(i,i+1)$ and $d_{N\delta}(i,i+1)$ connectivites involving $Asp^{134}-Pro^{135}$ and $Thr^{138}-Pro^{139}$ in the PAO peptide and $Arg^{138}-Pro^{139}$ in the KB7 peptide characterize *trans* configurations around these X−Pro peptide bonds. Conversely, a *cis* configuration around an X−Pro peptide bond would be characterized by $d_{\alpha\alpha}(i,i+1)$ and $d_{\alpha N}(i,i+1)$ connectivities which were not observed for these major resonances. The conformation of the minor resonances in the PAO and KB7 spectra could not be determined due to the small intensities of the peaks involved which produced no NOEs above the noise threshold in the NOESY spectrum. The fact that there is a significant amount of *cis* isomer in the PAK peptide around the $X-Pro^{139}$ but virtually no *cis* isomer around this same bond in the PAO and KB7 peptides may suggest that the *cis* isoform has less biological significance than the *trans* isomer in the PAO and KB7 pilin strains versus the PAK pilin strain.

3-D Structure Determination. Since a high population of the folded form of any peptide is needed before structure calculations can be meaningful, rough calculations were made to quantitate populations of the PAK, PAO, and KB7 peptides folded into turn conformations around the two sites spanned by residues Asp^{134}-X-X-Phe^{137} and Pro^{139}-X-Gly-Cys^{142}. With the understanding that accurate measurements of the folded form from a population of flexible peptides in solution are difficult to obtain, we have used a method developed by Yao *et al.* (1994) and adapted to estimate the turn population in the pilin peptides from the $^3J_{NH\alpha CH}$ coupling constants measured for the residues in position 2 of the two putative turns, i.e., residues X^{135} and X^{140}. A two-site model was used in which residues X^{135} and X^{140} could find themselves in either a turn conformation or in an extended conformation. Assuming 100% turn conformation, the coupling constants for X^{135} and X^{140} should be $^3J_{NH\alpha CH} = 4$ Hz, corresponding to a $\phi_2 = -60°$ (Pardi *et al.*, 1984). Assuming, 100% extended conformation, coupling constants of $^3J_{NH\alpha CH} = 9$ Hz are expected, corresponding to a $\phi < -100°$ (Pardi *et al.*, 1984). From these two extreme values of $^3J_{NH\alpha CH}$, the measured $^3J_{NH\alpha CH}$ values were used to estimate the percentage of turn or extended conformation for residues X^{135} and X^{140}, and these percentages were averaged and taken as a measure of the overall population of the folded peptide. Averaged values were obtained of 65% for the PAK peptide, 69% for the PAO peptide, and 75% for the KB7 peptide. Thus, from this rough estimate it would appear that about 70% of the population of the PAK, PAO, and KB7 peptides in solution is folded in solution.

Table 3: Constraints Used for Structure Generation of PAK, PAO, and KB7 128−144 Structures.

	PAK	PAO	KB7
NOE-derived distance constraints			
intraresidue	73	124	101
sequential ($\|i-j\|=1$)	62	66	52
medium range ($\|i-j\|<4$)	33	36	13
long range	1	8	1
total distance constraints	169	234	167
generic distance constraints	4	4	4
dihedral angle restraints			
ϕ	3	4	3
ψ	5	0	0

Using the SA/PEPFLEX-II protocol outlined in the Experimental Procedures section of this paper, the NMR solution structures of the PAO and KB7 peptides were calculated from NOEs, $^3J_{NH\alpha CH}$ coupling constants, and generic distance restraints (from measurement of temperature coefficients), and a solution structure of the PAK peptide previously determined in this laboratory (McInnes *et al.*, 1993) was refined under the same protocol. Table 3 presents a summary of the constraints used for the generation of the PAO, KB7, and PAK (McInnes *et al.*, 1993) peptides. An ensemble of 35 structures was generated for each peptide, and an average structure was calculated and energy minimized for a subset comprised of the major conformation within the ensemble. 25/35, 33/35, and 33/35 structures were used to calculate the averaged and minimized PAK, PAO, and KB7 structures, respectively.

Figure 4 shows the ensemble of simulated annealing structures and the energy-minimized average structure for the PAK, PAO, and KB7 peptides. Panels A, C, and E display the energy-minimized average structure of the PAK, PAO, and KB7 peptides, respectively, with the backbone displayed as a solid ribbon (red for PAO, green for PAK, and yellow for KB7) and the side chains CPK space-filled and color-coded. Panels B, D, and F display the ensemble of simulated annealing structures of the PAK, PAO, and KB7 peptides, respectively, with backbone atoms superimposed from residues 134 to 142 and the energy-minimized average structure of the backbone superimposed on the ensemble as a ribbon of congruent lines (red for PAO, green for PAK, and yellow for KB7).

Several features are evident from the ensemble of structures shown in Figure 4B,D,F. For all three peptides, there is generally a high degree of flexibility at the N- and C-termini (residues 128−134 and 142−144). The region between residues 134 and 142 shows the highest definition, as reflected in the calculated backbone RMSDs. The RMSDs for the superimposed residues within the disulfide loop (residues 129−142) are 1.2 ± 0.4, 1.2 ± 0.5, and 2.1 ± 0.2 for PAK, PAO, and KB7, respectively, whereas the backbone RMSDs calculated for superimposed residues 134−142 are 0.8 ± 0.2, 0.8 ± 0.3, and 1.4 ± 0.3 for PAK, PAO, and KB7, respectively.

Table 4 presents the ϕ, ψ values for the energy-minimized average structures of the PAK, PAO, and KB7 peptides. PROCHECK analyses of PAK, PAO, and KB7 structures show that none of the ϕ, ψ dihedral values fall into the disallowed range, with the majority of ϕ, ψ values falling into the most favored regions. One can clearly see from

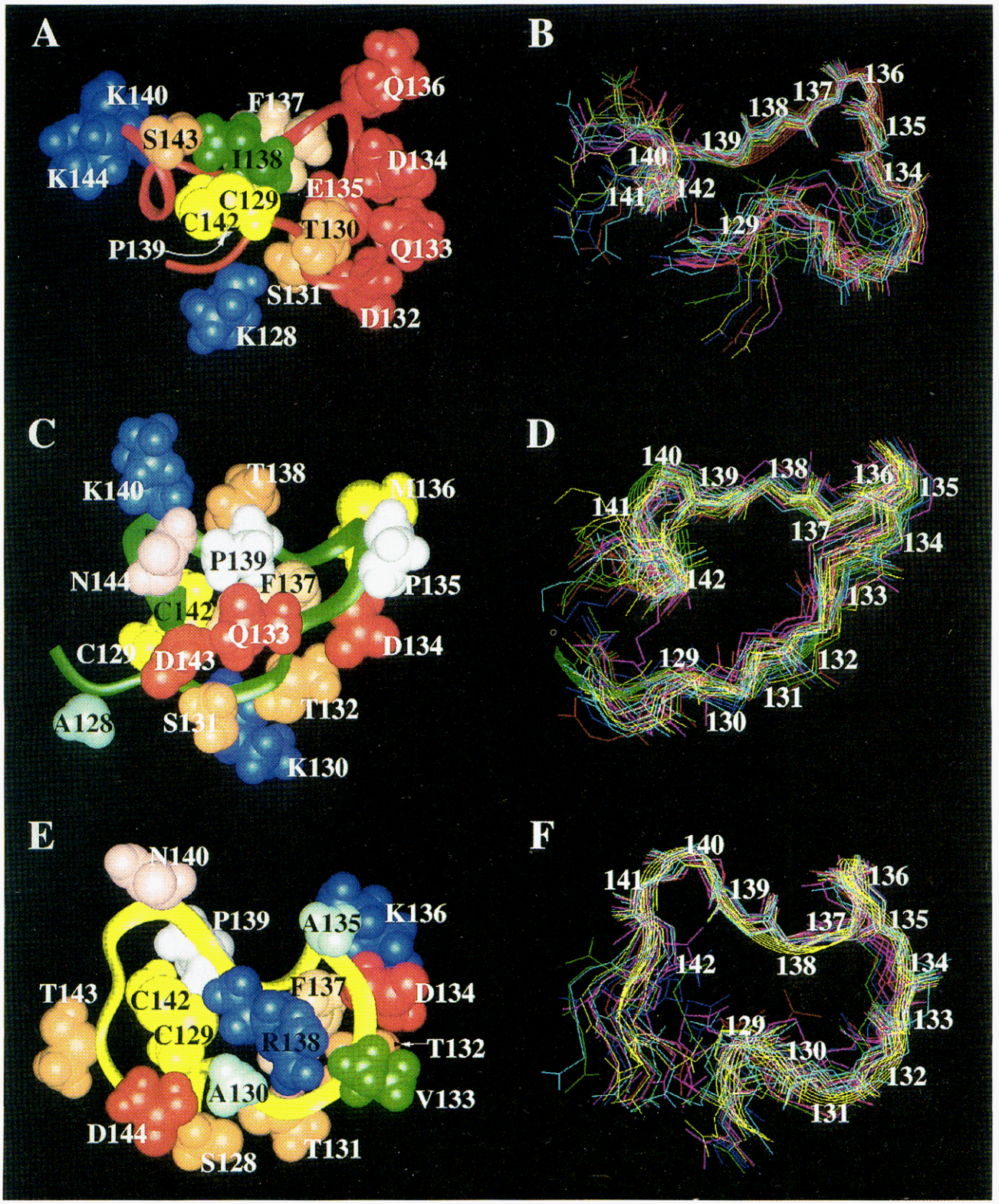

FIGURE 4: NMR solution structures of pilin peptides PAK 128−144 (top left and right), PAO 128−144 (middle left and right), and KB7 128−144 (bottom left and right). Panels A, C, and E display the energy-minimized average structure of the PAK, PAO, and KB7 peptides, respectively, with the backbone displayed as a solid ribbon (red for PAO, green for PAK, and yellow for KB7) and the side chains CPK space-filled and color-coded. Panels B, D, and F display the backbone atoms only from the ensemble of simulated annealing structures of the PAK, PAO, and KB7 peptides, respectively, with backbone atoms superimposed from residues 134 to 142. The backbone atoms of the energy-minimized average structure of each peptide are shown superimposed on the ensemble as a ribbon of congruent lines (red for PAO, green for PAK, and yellow for KB7).

the ϕ, ψ values presented in Table 4 that the backbone conformations of residues 130, 133, 135, 136, 138, 140, and 143 and the conserved residue Gly[141] are roughly similar, with residues 130, 133, 138, and 143 all in the extended ϕ, ψ dihedral space and residues 135, 136, 140, and Gly[141] within the conserved turn regions (discussed below). However, the backbone conformations of the other residues, which include residues 131 and 132 and conserved residues Cys[129], Asp[134], Phe[137], Pro[139], and Cys[142], vary across the strains, reflecting differences in the stereochemistry of the

Table 4: ϕ, ψ Values for the PAK, PAO, and KB7 128−144 Energy-Minimized Average Structures

	PAK		PAO		KB7	
residue	ϕ	ψ	ϕ	ψ	ϕ	ψ
128		142		98		149
129[a]	−80	−67	−109	153	−66	−52
130	−86	125	−76	129	−87	109
131	−69	−60	−86	96	−136	−68
132	−116	−78	−146	82	−88	134
133	−141	91	−84	102	−81	91
134	−112	76	−132	167	−158	141
135	−67	−37	−56	−40	−63	−39
136	−85	−20	−76	−22	−73	−14
137	−116	126	−80	150	−73	−54
138	−127	138	−107	105	−78	122
139	−72	167	−59	−42	−72	154
140	−66	116	−72	115	−73	114
141	96	3	105	−26	83	29
142	−81	−68	−111	−86	−81	149
143	−138	81	−134	107	−91	123
144	−139		−97		−89	

[a] Boldface indicates residues conserved in PAK, PAO, and KB7.

disulfide bond and in the disposition of hydrophobic residues across the strains. The differences in the backbone conformations of residue 132 and the conserved residue Asp[134] are reflected in the differences in the backbone proton chemical shifts observed for these residues (Table 1 and Figure 2A). The differences in the backbone conformations of the remaining residues are not clearly reflected in the backbone proton chemical shifts, especially in the cases of Cys[129] and Cys[142] for which the chemical shifts and $^3J_{NH\alpha CH}$ coupling constants are fairly similar and suggest an extended conformation. However, there is as yet no accepted methodology which allows intermediate chemical shifts or intermediate coupling constants (6 Hz < $^3J_{NH\alpha CH}$ < 8 Hz) to guide NMR solution structure determination, especially in the case of flexible peptides where there is likely to be an equilibrium of conformational states. Therefore, it is the NOEs, and especially the NOEs defining the hydrophobic cores of the PAK, PAO, and KB7 peptides, which ultimately determine the final conformation(s) of the peptides.

Panels A, C, and E of Figure 4 show the position of the side chains in the energy-minimized average structures of the PAK, PAO, and KB7 peptides, respectively. The PAK peptide (Figure 4A) shows a hydrophobic core composed of the side chains of Phe[137], Ile[138], and Pro[139], whereas the PAO peptide (Figure 4C) shows a hydrophobic core composed of the side chains of Phe[137] and Pro[139] but not Thr[138]. These hydrophobic interactions were observed as side-chain−side-chain NOEs between Phe[137], Ile[138], and Pro[139] in the PAK spectrum and between Phe[137] and Pro[139] in the PAO spectrum. Side-chain−side-chain NOEs between Phe[137] and Thr[138] were not observed in the PAO spectrum. A VADAR analysis of the PAK and PAO structures gives the fractional exposed surface area (FSA) of the side chains of each residue. The FSA values in the PAK peptide are 67%, 33%, and 34% for Phe[137], Ile[138], and Pro[139], respectively, whereas the comparative FSA values in the PAO peptide are 24%, 91%, and 39% for Phe[137], Thr[138], and Pro[139], respectively. These values suggest that the side chain of residue 138 is not as intimitely involved in the hydrophobic pocket in the PAO structure as it is in the PAK structure.

The KB7 peptide (Figure 4E) shows a different arrangement of hydrophobic residues. In this structure, a hydrophobic "face" is comprised of Val[133] and Phe[137], whereas the side chains of Arg[138] and Pro[139] are somewhat buried in the core of the peptide. The Val[133] and Phe[137] hydrophobic interaction is observed as side-chain−side-chain NOEs between these two residues in the KB7 spectrum. Side-chain−side-chain NOEs between Phe[137] and Pro[139] are not observed, although there are side-chain−side-chain NOEs between Arg[138] and Pro[139]. (Spectral overlap does not allow side-chain−side-chain NOEs to be cleanly observed between Phe[137] and Arg[138].) The VADAR analysis of the KB7 structure gives fractional surface area values of 81%, 38%, 36%, and 62% for Val[133], Phe[137], Arg[138], and Pro[139], respectively. These values suggest that the side chain of Phe[137] is also somewhat buried, mostly due to its disposition towards Val[133] which turns it toward the core of the peptide, whereas the side chain of Val[133] is fairly solvent exposed but still in close proximity to the side chain of Phe[137].

Figure 5 gives a picture of the positional definition of the side chains in the hydrophobic pockets of the PAK, PAO, and KB7 peptides. Panels A, D, and G show the variation in the disposition of side chains within the region encompassed by residues 134−142 for the PAK, PAO, and KB7 peptides, respectively, as represented by an ensemble of simulated annealing structures superposed over residues 134−142. The hydrophobic pocket of the PAK peptide (Figure 5A) appears fairly well defined, with the positions of the side chains of Phe[137], Ile[138], and Pro[139] well determined. The hydrophobic pocket of the PAO peptide (Figure 5D) appears slightly less well defined, with the position of the Phe[137] side chain slightly less well determined than it is in the PAK peptide. This could be a result of greater mobility in this region of the PAO peptide or of the absence of side-chain−side-chain NOEs from Phe[137] to residue 138 (Ile[138] in PAK and Thr[138] in PAO) in the PAO peptide. The position of the Phe[137] side chain in the KB7 peptide (Figure 5G) appears the least well determined of the three peptides, with the whole region from residues 134 to 142 appearing less well defined than it does in the PAK or PAO peptides. The lack of definition in this region of the KB7 peptide could be due to the fact that the hydrophobic face of KB7, comprised of Val[133] and Phe[137], is not completely included within the region superposed for the diagram. If folding of a peptide occurs around a nucleus of hydrophobic residues, then the area around a hydrophobic nucleus should be the least mobile region in the whole peptide with the greatest number of local side-chain contacts, leading to a greater number of local side-chain−side-chain NOEs and a structurally more defined region. Therefore, one would not expect the KB7 peptide to display the same level of side-chain or backbone definition for residues 134−142 as observed in the PAK or PAO peptides, since the hydrophobic nucleus of the KB7 peptide is not completely contained within this stretch of residues. Future relaxation studies are planned for the pilin peptides in order to differentiate between low structural definition as a result of genuine mobility of the backbone and side chains or low structural definition as a result of lack of NOE contacts or of averaging between static configurations.

Whereas structural differences are observed in the organization of the hydrophobic pockets of the PAK, PAO, and KB7 peptides, striking similarities are observed in the immediate vicinities of the β-turns, which are almost superimposable in terms of residue position and conformation. Figure 6 shows the energy-minimized average struc-

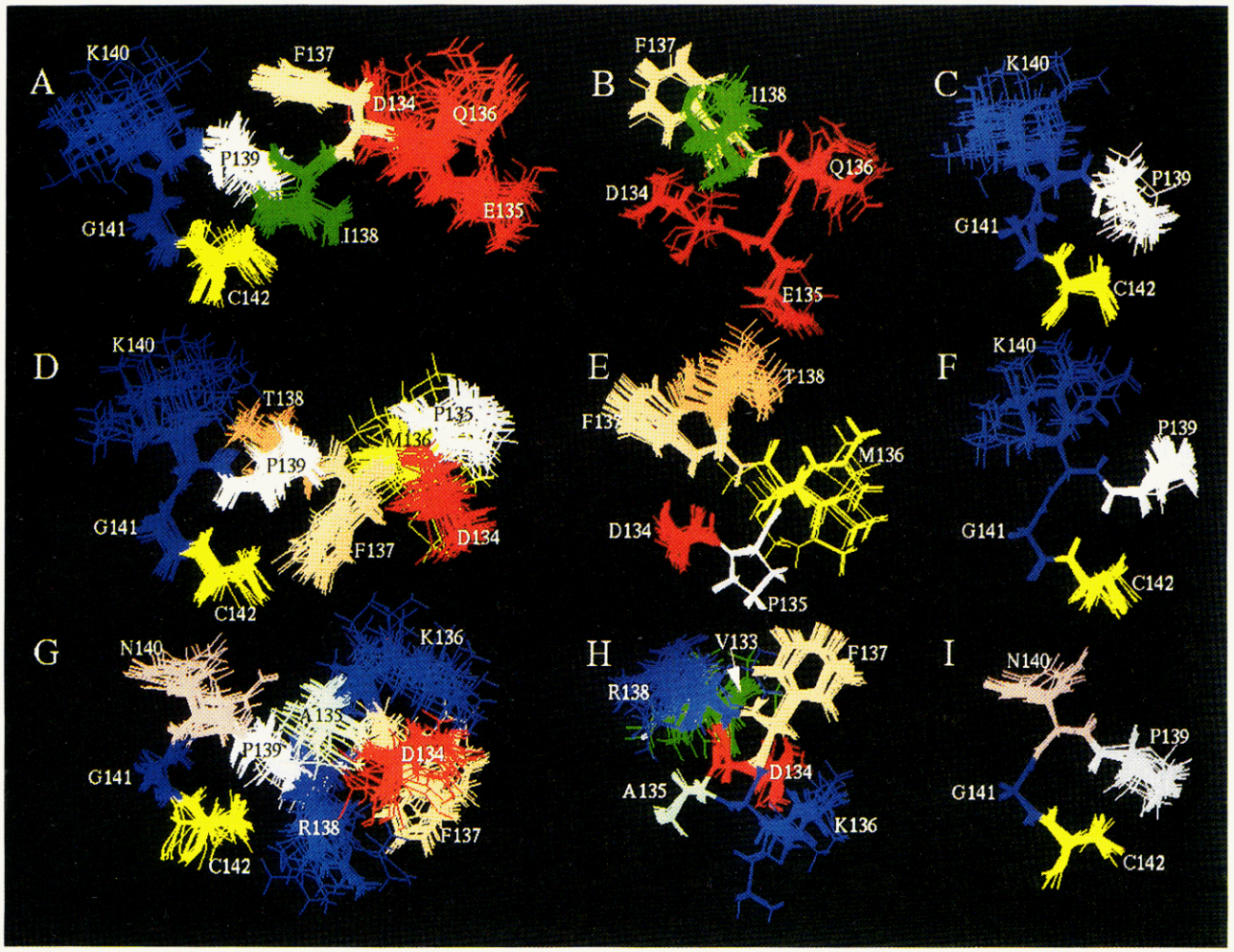

FIGURE 5: Ensemble of simulated annealing structures of pilin peptides PAK 128−144 (top strip of panels A, B, and C), PAO 128−144 (middle strip of panels D, E, and F), and KB7 128−144 (bottom strip of panels G, H, and I) showing the disposition of the side chains in the hydrophobic pockets and in the two β-turn regions. Panels A, D, and G show the disposition of side chains comprising the hydrophobic pockets for the PAK, PAO, and KB7 peptides, respectively, with backbone atoms superimposed from residues 134 to 142. Panels B, E, and H show the disposition of side chains in the first β-turn region (Asp^{134}-X-X-Phe^{137}) for the PAK, PAO, and KB7 peptides, respectively, with backbone atoms superimposed from residues 134 to 137. Panels C, F, and I show the disposition of side chains in the second β-turn region (Pro^{139}-X-Gly-Cys^{142}) for the PAK, PAO, and KB7 peptides, respectively, with backbone atoms superimposed from residues 139 to 142.

tures of PAK, PAO, and KB7 superimposed from residues 134−137 and 139−142 and displaying the structural similarity of the β-turn regions. For all three structures, two β-turns are observed between residues 134 and 142: a type I β-turn spanning the conserved sequence Asp^{134}-X-X-Phe^{137} and a type II β-turn in the conserved sequence Pro^{139}-X-Gly-Cys^{142}. The ϕ, ψ dihedral angles defining the turns fall within (−62 ± 6°, −39 ± 2°) (−78 ± 7°, −19 ± 5°) for $(\phi, \psi)_{135}$ $(\phi, \psi)_{136}$, and (−70 ± 4°, +115 ± 1°) (+95 ± 12°, +2 ± 28°) for $(\phi, \psi)_{140}$ $(\phi, \psi)_{141}$ (see Table 4), which agree with the concensus $(\phi, \psi)_2$ $(\phi, \psi)_3$ values of a type I and type II turn,[5] respectively, if one allows an error margin of ±20°.

VADAR analyses of the PAK, PAO, and KB7 structures detect the presence of H-bonds between Pro^{139} CO and Cys^{142} NH in all three structures, consistent with the presence of a β-turn in this region. Furthermore, additional H-bonds were found between Asp^{134} CO and Phe^{137} NH and between Thr^{138} CO and Cys^{142} NH in the PAO structure.[6] VADAR analysis of the PAK peptide assigned type I and type II turns for residues 134−137 and 139−142, respectively. The same regions in the PAO and KB7 peptides were assigned as type III[7] and type II turns.

The differences in the hydrophobic interactions between the three peptides account partly for the differences in the global folds of the backbones and in the relative orientation of the two β-turns. The differences in the relative orientations of the two β-turns can be seen in Figure 5A,D,G, where the position of the second β-turn (Pro^{139}-X-Gly-Cys^{142}) is kept fairly constant for each peptide, whereas the relative position of the the first β-turn (Asp^{134}-X-X-Phe^{137}) varies substantially for each peptide. This is clearly seen in the position of the side chains of Phe^{137} and Pro^{139} which are oriented very differently from figure to figure and which are reflected in the ϕ, ψ values of Phe^{137} and Pro^{139} (see Table 4).

[5] $(\phi, \psi)_2$ $(\phi, \psi)_3$ = (−60°, −30°) (−90°, 0°) for a type I turn and (−60°, +120°) (+90°, 0°) for a type II turn (Richardson, 1981).

[6] The identification of H-bonds in the VADAR program is based upon an ideal H−O length of 3.5 Å and an ideal CO−NH vector angle of 90°, with concessions for bent geometries which require closer proximity of the donor/acceptor pairs.

[7] The difference between a type I and type III turn is a subtle one involving the ψ_3 value only. The VADAR program assigns a type I turn when $-30° \leq \psi_3 \leq 0°$ and a type III turn when $0° \leq \psi_3 \leq +30°$.

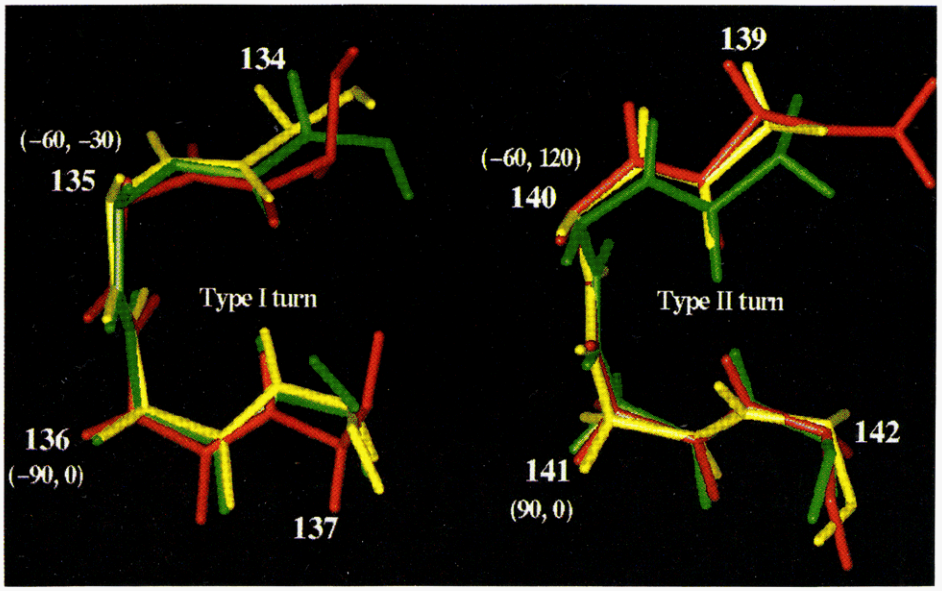

FIGURE 6: Energy-minimized average structures of PAK (red), PAO (green), and KB7 (yellow) superimposed from residues 134 to 137 (left) and residues 139 to 142 (right) showing the two β-turn regions.

Figure 5 gives a picture of the positional definition of the side chains around the two β-turn regions of the three peptides. Panels B, E, and H show the disposition of side chains in the first β-turn region (Asp[134]-X-X-Phe[137]) for the PAK, PAO, and KB7 peptides, respectively; and panels C, F, and I show the disposition of side chains in the second β-turn region (Pro[139]-X-Gly-Cys[142]) for the PAK, PAO, and KB7 peptides, respectively. The β-turn backbone conformations appear fairly well defined for each peptide. However, in Figure 5C two different conformations around the Gly[141] backbone for the PAK peptide can be seen, a function of the ψ_3 dihedral angle which "flip-flops" between $+20°$ or $-20°$ in the simulations. The positions of the side chains of hydrophilic residues in the turn regions of the three peptides are not especially well defined, suggesting the possibility of increased mobility for these residues. This can be observed in the side chain of residues 136 (Gln[136] in PAK, Met[136] in PAO, and Lys[136] in KB7) in the first β-turn region and 140 (Lys[140] in PAK and PAO and Asn[140] in KB7) in the second β-turn region where greater conformational flexibility could allow greater versatility in adapting to the topology of the receptor.

DISCUSSION

The Presence of β-Turns and Correlation to Antigenicity. From the wealth of X-ray crystal structures of antibody−peptide complexes which have recently emerged in the literature, it is clear that the most common antibody recognition motif in a peptide is a β-turn. This recognition motif is either a simple single type I or type II β-turn (Stanfield *et al.*, 1990; Rini *et al.*, 1992; Shoham, 1993) or a more complex arrangement of two or three turns, aligned sequentially along the recognition sequence of the peptide (Garcia *et al.*, 1992; Tormo *et al.*, 1994; Ghiara *et al.*, 1994). NMR studies of peptide antigens (Dyson *et al.*, 1985, 1988a,b; Chandrasekhar *et al.*, 1991; Blumenstein *et al.*, 1992; Scherf *et al.*, 1992; Zvi *et al.*, 1992; McInnes *et al.*, 1993; De Lorimier *et al.*, 1994) along with secondary structure predictions show that the peptide has a strong tendancy to adopt stable β-turn conformations in the absence of antibody. In fact, features incorporated into peptide antigens which stabilize β-turns have been shown to increase antibody affinity (Hinds *et al.*, 1991; Blumenstein *et al.*, 1992).

Recent crystallographic data obtained for antibody-antigen complexes show that antigens maintain β-turn conformations when bound while the antibody undergoes a conformational change in order to effect binding (Stanfield *et al.*, 1990; Rini *et al.*, 1992; Schulze-Gahmen *et al.*, 1993; Ghiara *et al.*, 1994). The study of a Fab in complex with a peptide from influenza virus hemagglutinin (Rini *et al.*, 1992; Schulze-Gahmen *et al.*, 1993) showed that while the antigen retains the free conformation (containing a type I β-turn), the antibody undergoes a large conformational change in one of the hypervariable loops to create a binding pocket for the β-turn of the peptide. A comparison of the crystal complexes of the principal neutralization site of HIV-1 with two Fab fragments, one from a broadly-neutralizing and one from a strain-specific antibody, found that the two Fab's recognized overlapping epitopes, while the HIV peptide antigen bound in both complexes as a conserved set of multiple β-turns (Ghiara *et al.*, 1994). The mechanism of antibody-induced fit as a means of antigen recognition allows a possible mechanism for cross-reactivity of the same antibody with different antigens or the same antigen with different antibodies. That the hypervariable loops in the combining sites of antibodies are capable of great flexibility in accommodating bound antigen allows for the possibility of the development of broad-spectrum vaccines against different strains of the same pathogen.

The β-turns in PAK, PAO, and KB7 occur in the receptor binding domain of the pilus. A strain-specific monoclonal antibody, PK99H, directed against the PAK pilus was found to block pilus-mediated adherence to buccal and tracheal epithelial cells (Doig *et al.*, 1990). The PK99H epitope was located in the sequence 134−140 (Asp-Glu-Gln-Phe-Ile-Pro-Lys) in PAK and was found to contain three critical residues, Phe[137], Ile[138], and Lys[140], two of which are located in the β-turns (Wong *et al.*, 1992). A second monoclonal antibody, PAK-13, raised against the PAK pilus is cross-reactive with

all three pilin peptides and their native pili and recognizes the same epitope in the PAK peptide as PK99H comprised of the same three critical residues (Phe^{137}, Ile^{138}, and Lys^{140}) (H. B. Sheth, W. Y. Wong, R. T. Irvin, and R. S. Hodges, unpublished results). These results confirm that the two β-turns, Asp^{134}-X-X-Phe^{137} and Pro^{139}-X-Gly-Cys^{142}, are the structural elements required for strain-specific or cross-reactive antibody recognition in the PAK peptide.

An examination of the energy-minimized average PAK structure in Figure 4A shows that the three critical residues for binding to antibody, Phe^{137}, Ile^{138}, and Lys^{140}, appear to be presented on one face of the molecule. A comparison of the PAK structure with the PAO and KB7 structures shows that the side chain of Phe^{137} is more buried in the PAO and KB7 structures and therefore less accessible for interaction with a combining site. In the KB7 structure in particular, the side chain of Phe^{137} is turned toward Val^{133} and toward another face of the molecule altogether. In addition, there are differences in the relative orientations of the two β-turns across the three peptide structures. These differences in turn orientation as well as in the position and surface accessibility of Phe^{137} observed in the PAK, PAO, and KB7 peptide structures suggest different binding topologies around the β-turns for each peptide. Different critical residues comprising the PAK-13 epitopes on the PAO and KB7 peptides (other than residues 137, 138, and 140 found critical for the PAK peptide−PAK-13 antibody interaction) might also be expected. A cross-reactive antibody like PAK-13 would therefore need a conformationally flexible combining site in order to accommodate such topologically different antigenic surfaces as those encountered with the PAK, PAO, and KB7 pilin peptides.

Whereas the hypervariable loops of a cross-reactive antibody like PAK-13 may change conformation to accommodate to different peptide configurations, it could also be argued that the peptides themselves change conformation to adapt to a more rigid antibody combining site. However, transferred NOE studies of the PAK, PAO, and KB7 peptides binding to the Fab fragment of PAK-13 (unpublished data) show no change in secondary conformation of the peptides upon binding to antibody. This suggests that the secondary conformation of the turns as well as the relative orientations of the turns is maintained upon binding to antibody, in agreement with the crystallographic studies (Rini *et al.*, 1992; Schulze-Gahmen *et al.*, 1993).

Implications of the Structure of PAK and KB7 Peptides for Receptor Binding. PAK and KB7 pilin C-terminal peptides have been demonstrated to bind with similar affinity to their receptor on host cells (A549 human pneumocyte cell line) (Wong *et al.*, 1995). This occurs despite limited sequence homology between the two strains. Wong *et al.* (1995) have mapped the adhesintope of PAK binding to A549 cells (i.e., the residues which are essential for affinity) using a series of peptides incorporating single alanine replacement. The essential residues identified for PAK were Ser^{131}, Gln^{136}, Ile^{138}, Pro^{139}, Gly^{141}, and Lys^{144}. In addition, the disulfide loop between residues Cys^{129} and Cys^{142} was shown to be required for recognition of the peptide by the receptor. Data obtained for KB7 adherence to A^{549} indicates that Ala^{130}, Thr^{131}, Thr^{132}, Val^{133}, Asp^{134}, Ala^{135}, Lys^{136}, Arg^{138}, and Pro^{139} are essential residues.

Interestingly, the residue position in the sequence appears to determine the adhesintype rather than identity of residue type. For example, the positions common to both adhesintopes are 131, 136, 138, and 139, yet 136 involves glutamine in PAK and lysine in KB7 and 138 involves isoleucine in PAK and arginine in KB7. These results lead to the proposal by Wong *et al.* (1995) of multiple compensational mutations between strains which may be required to maintain the structural requirements for receptor interactions. For example, though the essential Ile^{138} in PAK is replaced by the essential Arg^{138} in KB7, the hydrophobicity for receptor binding is maintained by the essential residue Val^{133} in KB7. Similarly, the positive charge of Lys^{144} in PAK which is Asp^{144} in KB7 could be replaced by Arg^{138} or Lys^{136} in KB7.

Can a comparison of the solution structures obtained for the PAK and KB7 pilin peptides explain their similar receptor binding affinities? As has already been established, the backbone conformations of PAK and KB7 are very similar in the regions of the two β-turns. From the adhesintope mapping results, three of the six essential residues in the PAK sequence, and four of the nine essential residues in the KB7 sequence lie in the region encompassing the two turns. Thus, it would seem as if the region of the two β-turns constitutes the important structural motif required for receptor binding.

For the PAK peptide, two out of the four essential residues, Pro^{139} and Gly^{141}, are located in the i and $i+2$ positions of the second type II β-turn (Pro^{139}-X-Gly-Cys^{142}). Therefore, it is possible that the second type II β-turn is the important structural motif required for receptor binding. Since the second type II turn is present in the *cis* isoform of PAK (McInnes *et al.*, 1994), then it is possible that this form binds to the receptor. The lack of the *cis* isomer in KB7, however, seems to suggest that the *trans* isomers are responsible for receptor binding although the rotation of the Arg^{138}−Pro^{139} amide bond could occur upon binding. The importance of the first type I β-turn between Asp^{134}-X-X-Phe^{137} for PAK peptide receptor binding is less clear since only one of the adhesintope residues (Gln^{136} in position $i+2$) is required for receptor binding. However, it is possible that the PAK peptide binds in a double-turn motif, with the second turn being more intimately associated with the receptor.

For the KB7 peptide, the situation is somewhat reversed, since three of the nine essential residues are located in the the first type I β-turn and only one is in the second type II β-turn. Asp^{134}, Ala^{135}, and Lys^{136} are located at the i, $i+1$ and $i+2$ positions of the type I β-turn, whereas Pro^{139} is located at the i position of the type II β-turn. Wong *et al.* (1995) found that substitution of Gly^{141} in the KB7 sequence still allowed binding to A549 cells, suggesting that the type II β-turn is not as essential for interaction to the receptor. Furthermore, more of the adhesintope residues were located at the N-terminal side of the KB7 peptide and close to the type I β-turn. This all suggests that the type I β-turn is more important than the type II β-turn for the KB7 pilin peptide interaction with its receptor, although it is also possible that the KB7 peptide binds in a double-turn motif, with the first turn being more intimately associated with the receptor.

It is not surprising that the residues comprising the adhesintopes of the PAK and KB7 peptides are so different given that the overall folds of these two peptides differ so markedly as well as the disposition of the side chains comprising the hydrophobic pockets. The adhesintope of the PAK peptide seems to center around its hydrophobic pocket, comprised of the side chains of Phe^{137}, Ile^{138}, and Pro^{139}; whereas the adhesintope of the KB7 peptide seems

to center around its hydrophobic face, comprised of the side chains of Val^{133} and Phe^{137}. In fact, with the exception of Phe^{137}, these hydrophobic residues consitutute some of the most important residues in the adhesintopes of both peptides.

The relative orientation of the two β-turns is apparently not significant for binding. This can be deduced since the turn orientation in the two strains is quite different, though the peptides may undergo a conformational change upon binding in order to effect a more favorable orientation of the turns for receptor affinity. Since Phe^{137} is nonessential in both the PAK and KB7 peptides for receptor binding, it is unlikely that the hydrophobic stacking of Phe^{137} and Pro^{139} is important. This suggests that the interaction is broken in the bound form of PAK and possibly assumes a conformation that resembles that of KB7. If PAK binds as the *cis* form, then this conformational rearrangement may not be necessary. Other residues which have been shown to constitute part of the adhesintope, such as Ser^{131} and Lys^{144} in PAK, are found in less structured regions of the peptide. They may not contribute to receptor affinity in terms of stabilization of secondary structure.

Implications for Synthetic Vaccine Design. One of the goals in the development of synthetic vaccines is to engineer a peptide immunogen which optimizes the desired immunological response. The discovery in recent years that immunogenic and antigenic peptides adopt stable and thus identifiable secondary structure in solution brings this goal within reach. In the case of *P. aeruginosa*, the identification of a common structural motif consisting of two β-turns in the receptor binding domains of PAK, PAO, and KB7 pilin peptides suggests that it is the turns which constitute the critical structural element for receptor binding. This finding coupled with the observation that β-turns occur in immunogenic regions of peptides and proteins and that their structure is preserved upon antibody binding indicates that peptide engineering of synthetic vaccines might be used to generate peptides with increased stability of the β-turn structural elements. A more stable β-turn in the synthetic vaccine should lead to enhanced immunogenicity and cross-reactivity of resulting antibodies produced from the vaccine.

Though this NMR study has identified a common structural motif among three peptide antigens from the receptor binding domain of three strains of *P. aeruginosa* pilin, it has also found that the overall folds of the three peptide antigens differ as well as the disposition of side chains comprising the hydrophobic pockets. These latter results indicate the complexity of the structure–function relationships involved in the binding of *P. aeruginosa* strains to their receptor and the need for more three-dimensional structures of the receptor binding domains of other strains and analogs of these native peptides. Such studies in conjunction with adhesintope mapping and immunological studies should be able to determine the role side chains play in maintaining the folded structure versus their role in controlling specificity of the immune response in generating *P. aeruginosa* anti-peptide antibodies that are cross-reactive and strain-specific.

ACKNOWLEDGMENT

The authors thank Paul Semchuck for peptide synthesis, purification, and mass spectrometry, Robert Boyko, Tim Jellard, and Leigh Willard for computer programming assistance, and Drs. Frank Sönnichsen, David Wishart, and Jianjun Wang for helpful discussions.

REFERENCES

Baker, N., Hansson, G. C., Leffler, H., Riise, G., & Svanbord-Eden, C. (1990) *Infect. Immun. 58*, 2361–2366.

Bax, A., & Davis, D. G. (1985) *J. Magn. Reson. 65*, 355–360.

Billeter, M., Braun, W., & Wüthrich, K. (1982) *J. Mol. Biol. 155*, 321–346.

Blumenstein, M., Matsueda, G. R., Timmons, S., & Hawiger, J. (1992) *Biochemistry 31*, 10692–10698.

Brown, S. C., Weber, P. L., & Mueller, L. (1988) *J. Magn. Reson. 77*, 166–169.

Cahn, R. S., Ingold, C. K., & Prelog, V. (1956) *Experientia 12*, 81–94.

Chandrasekhar, K., Profy, A. T., & Dyson, H. J. (1991) *Biochemistry 30*, 9187–9194.

De Lorimier, R., Moody, M. A., Haynes, B. F., & Spicer, L. D. (1994) *Biochemistry 33*, 2055–2062.

Doig, P., Smith, N. R., Todd, T., & Irvin, R. T. (1987) *Infect. Immun. 55*, 1517–1522.

Doig, P., Todd, T., Sastry, P. A., Lee, K. K., Hodges, R. S., Paranchych, W., & Irvin, R. T. (1988) *Infect. Immun. 56*, 1641–1646.

Doig, P., Sastry, P. A., Hodges, R. S., Lee, K. K., Paranchych, W., & Irvin, R. T. (1990) *Infect. Immun. 58*, 124–130.

Dyson, H. J., Cross, K. J., Houghten, R. A., Wilson, I. A., Wright, P. E., & Lerner, R. A. (1985) *Nature 318*, 480–483.

Dyson, H. J., Rance, M., Houghten, R. A., Lerner, R. A., & Wright, P. E. (1988a) *J. Mol. Biol. 201*, 161–200.

Dyson, H. J., Rance, M., Houghten, R. A., Wright, P. E., & Lerner, R. A. (1988b) *J. Mol. Biol. 201*, 201–217.

Gagné, S. M., Tsuda, S., Li, M. X., Chandra, M., Smillie, L. B., & Sykes, B. D. (1994) *Protein Sci. 3*, 1961–1974.

Garcia, K. C., Ronco, P. M., Verroust, P. J., Brunger, A. T., & Amzel, L. M. (1992) *Science 257*, 502–507.

Ghiara, J. B., Stura, E. A., Stanfield, R. L., Profy, A. T., & Wilson, I. A. (1994) *Science 264*, 82–85.

Hinds, H. G., Welsh, J. H., Brennand, D. M., Fisher, J., Glennie, M. J., Richards, H. G. J., Turner, D. L., & Robinson, J. A. (1991) *J. Med. Chem. 34*, 1777–1789.

Irvin, R. T. (1993) in *Pseudomonas aeruginosa as an opportunistic pathogen* (Campa, M., Ed.) Plenum Press, New York.

Irvin, R. T., Doig, P., Lee, K. K., Sastry, P. A., Paranchych, W., Todd, T., & Hodges, R. S. (1989) *Infect. Immun. 57*, 3720–3726.

Jeener, J., Meier, B. H., Bachmann, P., & Ernst, R. R. (1979) *J. Chem. Phys. 71*, 4546–4553.

Karplus, M. (1963) *J. Am. Chem. Soc. 85*, 2870–2871.

Krivan, H. C., Ginsburg, V., & Roberts, D. D. (1988a) *Arch. Biochem. Biophys. 260*, 493–496.

Krivan, H. C., Roberts, D. D., & Ginsburg, V. (1988b) *Proc. Natl. Acad. Sci. U.S.A. 85*, 6157–6161.

Kuntz, I. D. (1972) *J. Am. Chem. Soc. 94*, 4009–4012.

Laskowski, R. A., MacArthur, M. W., Moss, D. S., & Thornton, J. M. (1993) *PROCHECK v.2.1.4, Program to check the stereochemical quality of protein structures*, Oxford Molecular, Oxford.

Lee, K. K., Doig, P., Irvin, R. T., Paranchych, W., & Hodges, R. S. (1989) *Mol. Microbiol. 3*, 1493–1499.

Lee, K. K., Paranchych, W., & Hodges, R. S. (1990) *Infect. Immun. 58*, 2727–2732.

Lee, K. K., Sheth, H. B., Wong, W. Y., Sherburne, R., Paranchych, W., Hodges, R. S., Lingwood, C. A., Krivan, H., & Irvin, R. T. (1994) *Mol. Microbiol. 11*, 705–713.

Lee, K. K., Wong, W. Y., Sheth, H. B., Hodges, R. S., Paranchych, W., & Irvin, R. T. (1995) *Methods Enzymol. 253*, 115–131.

Macura, S., & Ernst, R. R. (1980) *Mol. Phys. 41*, 95–117.

McInnes, C., Sönnichsen, F. D., Kay, C. M., Hodges, R. S., & Sykes, B. D. (1993) *Biochemistry 32*, 13432–13440.

McInnes, C., Kay, C. M., Hodges, R. S., & Sykes, B. D. (1994) *Biopolymers 34*, 1221–1230.

Nilges, M., Clore, G. M., & Gronenborn, A. M. (1988) *FEBS Lett. 229*, 317–324.

Nilges, M., Clore, G. M., & Gronenborn, A. M. (1990) *Biopolymers 29*, 813–822.

Paranchych, W., Sastry, P. A., Volpel, K., Loh, B. A., & Speert, D. P. (1986) *Clin. Invest. Med. 9*, 113−118.
Paranchych, W., Pasloske, B. L., & Sastry, P. A. (1990) in *Pseudomonas: Biotransformations, Pathogenesis and Evolving Biotechnology* (Sliver, S., Chakrabarty, A. M., Iglewski, B. B. H., & Kaplan, S., Eds.) pp 342−351, American Society for Microbiology, Washington, DC.
Pasloske, B. L., Sastry, P. A., Finlay, B. B., & Paranchych, W. (1988) *J. Bacteriol. 170*, 3738−3741.
Piatini, U., Sorenson, O. W., & Ernst, R. R. (1982) *J. Am. Chem. Soc. 104*, 6800−6801.
Pier, G. B. (1985) *J. Infect. Dis. 151*, 575−580.
Ramphal, R., Sadoff, J. C., Pyle, M., & Silipigni, J. D. (1984) *Infect. Immun. 44*, 38−40.
Ramphal, R., Carnoy, C., Fievre, S., Michalski, J.-C., Houdret, N., Lamblin, G., Strecker, G., & Roussel, P. (1991) *Infect. Immun. 59*, 700−704.
Rance, M., Sorenson, O. W., Bodenhausen, G., Wagner, G., Ernst, R. R., & Wüthrich, K. (1983) *Biochem. Biophys. Res. Commun. 117*, 479−485.
Richardson, J. S. (1981) *Adv. Protein Chem. 34*, 167−339.
Rini, J. M., Schulze-Gahmen, U., & Wilson, I. A. (1992) *Science 255*, 959−965.
Rivera, M., & Nicotra, M. B. (1982) *Am. Rev. Respir. Dis. 126*, 833−836.
Rose, G. D., Gierasch, L. M., & Smith, J. A. (1985) *Adv. Protein Chem. 37*, 1−107.
Sajjan, U., Reisman, J., Doig, P., Irvin, R. T., Forstner, G., & Forstner, J. (1991) *J. Clin. Invest. 89*, 657−665.
Scherf, T., Hiller, R., Naider, F., Levitt, M., & Anglister, J. (1992) *Biochemistry 31*, 6884−6897.
Schulze-Gahmen, U., Rini, J. M., & Wilson, I. A. (1993) *J. Mol. Biol. 234*, 1098−1118.
Sheth, H. B., Lee, K. K., Wong, W. Y., Srivastava, G., Hindsgaul, O., Hodges, R. S., Paranchych, W., & Irvin, R. T. (1994) *Mol. Microbiol. 11*, 715−723.
Shohan, M. (1993) *J. Mol. Biol. 232*, 1169−1175.
Stanfield, R. L., Fieser, T. M., Lerner, R. A., & Wilson, I. A. (1990) *Science 248*, 712−719.
States, D. J., Haberkorn, R. A., & Ruben, D. J. (1982) *J. Magn. Reson. 48*, 286−292.
Todd, T. R. J., Franklin, A., Mankinen-Irvin, P., Gurman, G., & Irvin, R. T. (1989) *Am. Rev. Respir. Dis. 140*, 1585−1589.
Tormo, J., Blass, D., Parry, N. R., Rowlands, D., Stuart, D., & Fita, I. (1994) *EMBO J. 13*, 2247−2256.
Wagner, G., Neuhaus, D., Wörgötter, E., Vasák, M., Kägi, J. H. R., & Wüthrich, K. (1986) *J. Mol. Biol. 187*, 131−135.
Wang, J., Hodges, R. S., & Sykes, B. D. (1995) *J. Am. Chem. Soc. 117*, 8627−8634.
Wishart, D. S., Sykes, B. D., & Richards, F. M. (1991) *J. Mol. Biol. 222*, 311−333.
Wong, W. Y., Irvin, R. T., Paranchych, W., & Hodges, R. S. (1992) *Protein Sci. 1*, 1308−1318.
Wong, W. Y., Campbell, A. P., McInnes, C., Sykes, B. D., Paranchych, W., Irvin, R. T., & Hodges, R. S. (1995) *Biochemistry 34*, 12963−12972.
Wüthrich, K. (1986) in *NMR of Proteins and Nucleic Acids*, John Wiley and Sons, New York.
Wüthrich, K., Billeter, M., & Braun, W. (1984) *J. Mol. Biol. 180*, 715−740.
Yao, J., Feher, V. A., Espejo, B. F., Reymond, M. T., Wright, P. E., & Dyson, H. J. (1994) *J. Mol. Biol. 243*, 736−753.
Zvi, A., Hiller, R., & Anglister, J. (1992) *Biochemistry 31*, 6972−6979.

BI951076O